

Brain acetylhydrolase that inactivates platelet-activating factor is a G-protein-like trimer

Yew S. Ho, Lora Swenson*, Urszula Derewenda, Laurence Serre*†, Yunyi Wei, Zbyszek Dauter‡, Mitsuharu Hattori§, Tomoya Adachi§, Junken Aoki§, Hiroyuki Arai§, Keizo Inoue§ & Zygmunt S. Derewenda

Department of Molecular Physiology and Biological Physics, University of Virginia Health Sciences Center, PO Box 10011, 1300 Jefferson Park Avenue, Charlottesville, Virginia 22906-0011, USA

* Department of Biochemistry, University of Alberta, Edmonton, Alberta T6G 2H7, Canada

‡ EMBL Outstation, 22603 Hamburg, Germany

§ Department of Health Chemistry, Faculty of Pharmaceutical Sciences, The University of Tokyo, Hongo 7-3-1, Bunkyo-ku, Tokyo 113, Japan

THE platelet-activating factor PAF (1-*O*-alkyl-2-acetyl-*sn*-glycero-3-phosphocholine) is a potent lipid first messenger active in general cell activation, fertilization, inflammatory and allergic reactions, asthma, HIV pathogenesis, carcinogenesis, and apoptosis¹⁻⁵. There is substantial evidence that PAF is involved in intracellular signalling, but the pathways are poorly understood. Inactivation of PAF is carried out by specific intra- and extracellular acetylhydrolases⁶ (PAF-AHs), a subfamily of phospholipases A₂ that remove the *sn*-2 acetyl group. Mammalian brain contains at least three intracellular isoforms, of which PAF-AH(Ib) is the best characterized⁷⁻⁹. This isoform contains a heterodimer of two homologous catalytic subunits α_1 and α_2 , each of relative molecular mass 26K, and a non-catalytic 45K β -subunit, a homologue of the β -subunit of trimeric G proteins. We now report the crystal structure of the bovine α_1 subunit of PAF-AH(Ib) at 1.7 Å resolution in complex with a reaction product, acetate. The tertiary fold of this protein is closely reminiscent of that found in p21^{ras} and other GTPases. The active site is made up of a trypsin-like triad of Ser 47, His 195 and Asp 192. Thus, the intact PAF-AH(Ib) molecule is an unusual G-protein-like (α_1/α_2) β trimer.

Mammalian brain contains significant levels of PAF, which acts as a synapse messenger and transcription inducer of the early-response genes *c-fos* and *c-jun*¹⁰. It accumulates rapidly in neural tissue during seizures or ischaemia¹¹ and the resulting brain damage can be reduced by PAF antagonists¹². PAF is also being implicated as a messenger in long-term potentiation, a cellular model of memory formation¹³. The β -subunit of the PAF-AH(Ib) complex is a product of the gene that is responsible for the onset of type-1 lissencephaly, a developmental brain disorder caused by impaired neuronal migration, in which no cortex is formed¹⁴. This suggests a potential role for PAF in early brain development and neuronal migration.

The two catalytic α -subunits of PAF-AH(Ib) (this new notation is consistent with that accepted for the structurally related G-protein subunits) share extensive amino-acid sequence identity—63% in the bovine form⁹—but the consensus sequence they share is unique among proteins. When these subunits are purified or overexpressed individually in *Escherichia coli*, they form catalytically competent homodimers. *In vivo*, however, α_1 is preferentially labelled by [1,3-³H]diisopropyl fluorophosphate in the heterodimer, suggesting functional asymmetry⁹.

The PAF-AH(Ib) α_1 subunit is a single polypeptide chain of 231 residues⁷. The molecule contains a single α/β domain with a central, parallel, 6-stranded β -sheet. This fold is very like that found in GTPases (Fig. 1a, 2). The insertions and deletions in the

† Present address: Institut de Biologie Structurale (IBS), Avenue des Martyrs, 38042 Grenoble Cedex, France.

α_1 structure, compared to p21^{ras}, can be rationalized in functional terms: for example, the turn/ β_1 fragment unique to p21^{ras} and involved in GTP binding is absent in α_1 , and the first β -strand found in the α -subunit of the G protein transducin and in p21^{ras}, which is involved in interactions with other proteins, is also unique to these proteins. On the other hand, α_1 contains a unique N-terminal α -helix which, together with the loop that follows, is part of the dimer-forming interface. Finally, the catalytic centre of α_1 is located on two Ω loops that are significantly different from their analogues in p21^{ras}.

Serine 47 has been identified as the putative nucleophile⁷. In the crystal structure, Ser 47 is close to His 195; further, the imidazole ring of His 195 is hydrogen-bonded through its N δ 1 atom to the side-chain carboxyl of Asp 192 (Fig. 1b). The stereochemistry of this triad is indicative of a catalytic function, which is supported by the inactivity of H195A and D192N mutants (data not shown). The chirality of the triad is the same as that found in the active sites of other esterases and neutral lipases, where nucleophilic attack is on the *re* face of the ester¹⁵ (the Cahn–Ingold–Prelog nomenclature specified the topologically different faces of peptides and esters involved in nucleophilic attack as *re* faces, not *re* and *si*¹⁵). The acetate bound in the active site interferes with the ground-state stereochemistry of the triad and disrupts the hydrogen bond that should link His 195 and Ser 47 in the active enzyme. The bound acetate also makes it possible to identify unambigu-

ously the hydrogen-donor groups that constitute the oxyanion hole: the main-chain amides of Ser 47 and Gly 74, and N δ 1 amide of Asn 104 (Fig. 1b). Cloned human plasma PAF-AH is also thought to work by means of a catalytic triad¹⁶.

The α_1 homodimer is formed by two molecules related by the crystallographic two-fold axis (Fig. 3a), oriented so that the carboxyl edges of their β -sheets are close to one another. In each monomer, a total of 1,150 \AA^2 of solvent-accessible surface is lost when the dimer forms (Fig. 3b); 18 amino acids lose more than 20 \AA^2 upon dimerization, and fourteen of these are conserved between the two catalytic subunits. Of the remaining four, only C55Y is a non-conservative substitution; this rationalizes the disorder between residues 53–56 (see Methods). Many of the interface-forming residues are hydrophilic and numerous hydrogen bonds and salt bridges mediate the contacts: for example, Gln 18–His 106, Asp 20–Arg 41, Ser 25–Gln 143 and Arg 29–Tyr 193; there are no buried water molecules within the interface.

The conserved character of the interface-forming residues indicates that the crystallographic dimer described here is a good model for the *in vivo* α_1/α_2 heterodimer. It is a doughnut-shaped structure with a solvent-accessible gorge, some 15 \AA deep. The two active sites are at the bottom of the gorge and only 12 \AA from each other, as measured between the carboxyl carbons of the acetate. The proximity suggests that these sites do not function independently, consistent with the noted functional asymmetry of



FIG. 1 a, A stereo plot of α -carbon atoms of the final model; the residues that form the catalytic triad are shown in their entirety and are labelled. b, An 'omit' difference electron density map showing active-site residues (labelled) and the acetate molecule (Ace) after all these groups were deleted from phase calculation and the remainder of the protein was subjected to two cycles of crystallographic refinement using PROLSQ. The electron density is contoured at a 2σ level.

the heterodimer in which the activity of the α_2 subunit can be suppressed by steric effects.

In general catalysis by neutral lipases and secretory phospholipases A2 is markedly enhanced at substrate concentrations above their critical micellar concentrations (CMCs): plasma PAF-AH is significantly more active at PAF concentrations (CMC_{PAF} , 1.1 μ M) above 5 μ M (ref. 6). The structure of the α_1 homodimer shows that the entrance to the active gorge is not particularly hydrophobic, and there is no flexible secondary structure element that might function as a 'lid', a structural motif in serine-dependent lipases that are active at interfaces¹⁷. The crystal structure is therefore consistent with the enzyme being active on a monomeric substrate.

The activity of all PAF-AHs depends on their recognition of a

short acyl chain in the *sn*-2 position, but stringency varies between different isoforms. The plasma enzyme prefers the *sn*-2 acetyl group but will hydrolyse acyl chains of up to five carbons¹⁸; the brain isoform II also has broader specificity¹⁹. However, PAF-AH(Ib) is very selective, being 20 times less active towards propionyl-PAF than PAF itself¹⁹. The crystal structure can explain these effects. Three residues, all conserved in the α_2 subunit, come into contact with the acetate's methyl group: they are Leu 48, Leu 194 and Thr 103 (Fig. 4). Each donates one methyl group, that is, at C δ 1 (Leu 194), C δ 2 (Leu 48) and C γ 2 (Thr 103), to form a hydrophobic pocket for the substrate's acetyl moiety. Analysis of the probe-accessible surface created by these groups, and structural comparison with other neutral lipases indicate that the

FIG. 2 A comparison of the tertiary structures of PAF-AH(Ib) α_1 and GTPases: a, p21^{ras} (entry 5P21 in the Protein Data Bank); b, α_1 subunit of PAF-AH(Ib); c, catalytic domain of the transducin α -chain (entry 1GIA). Red, C α atoms used for least-squares overlap of PAF-AH(Ib) α_1 with either of the GTPases; green, the most significant insertions or deletions; blue, the partly disordered residues (55–61) in PAF-AH(Ib) α_1 . Figure generated using RIBBONS (M. Carson). Secondary structure elements of PAF-AH(Ib) α_1 : H0, residues 22 to 36; H1, 47 to 55; H2, 77 to 90; H3, 110 to 127; H4, 147 to 164; H5, 198 to 215; S1, 41 to 45; S2, 67 to 70; S3, 96 to 101; S4, 131 to 136; S5, 169 to 173.

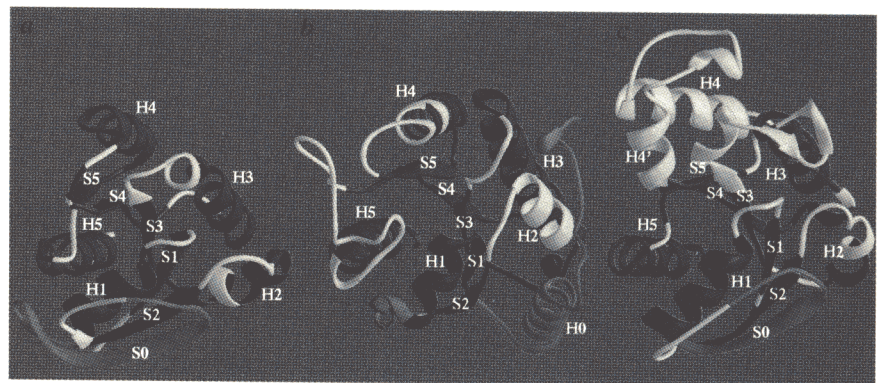


TABLE 1 Summary of crystallographic analysis

X-ray data collection	Native	Mercury	Lead	Gold	Cryo
Beam line (λ)	BW7B (0.895)	X31 (0.95)	X31 (0.93)	X31 (0.95)	BW7B (0.895)
Temperature	RT	RT	RT	RT	120 K
Total reflections	86,304	201,462	68,970	122,863	387,544
Unique reflections	17,228	15,029	13,983	15,006	33,716
Resolution range (\AA)	20–2.1	20–2.19	20–2.24	20–2.20	20–1.65
Completeness (%)	99.8	100	98.9	99.9	99.7
R_{sym} (%)*	8.4	8.2	9.1	7.3	6.3
R_{iso} (%)†	–	11.9	17.2	15.6	–
Overall phasing results					
R_{cullis} (acentric/centric)‡		0.83/0.76	0.81/0.76	0.88/0.85	
Phasing power (acentric/centric)§		1.20/0.90	1.30/0.80	0.80/0.50	
Number of sites (major/minor)		1/2	2/3	2/4	
Final refinement results (120 K) (data in parenthesis relate to a Δ 55–61 model)					
Resolution limit				8.5–1.7 \AA	
R_{factor} (%)				0.174 (0.195)	
Bond distance (1–2) r.m.s.				0.024 (0.015)	
Angle distance (1–3) r.m.s.				0.044 (0.034)	
Planar (1–4) r.m.s.				0.060 (0.047)	
Peptide planes r.m.s.				8.0° (5.7°)	
Main-chain average B-factor/r.m.s.				20.3 \AA^2 /1.4 \AA^2	
Side-chain average B-factor/r.m.s.				25.9 \AA^2 /3.1 \AA^2	
Residues in most favoured regions of Ramachandran plot¶				90.6%	
Residues in additional allowed regions				8.8%	

RT, room temperature

* $R_{\text{sym}} = \sum |I_i - \langle I \rangle| / \sum I_i$, where I_i is the intensity of the i th observation and $\langle I \rangle$ is the mean intensity of the reflection.

† $R_{\text{iso}} = \sum |F_{\text{PH}} - F_{\text{P}}| / \sum |F_{\text{P}}|$, where F_{P} and F_{PH} are the structure factor amplitudes for native and derivative crystals respectively.

‡ $R_{\text{cullis}} = \sum |\epsilon| / \sum |F_{\text{PH}} - F_{\text{P}}|$.

§ Phasing power = $\langle F_{\text{H}} \rangle / \langle \epsilon \rangle$, where $\langle F_{\text{H}} \rangle$ is the mean heavy-atom contribution and $\langle \epsilon \rangle$ is the mean lack of closure.

|| $R_{\text{factor}} = \sum |F_{\text{obs}} - F_{\text{calc}}| / \sum |F_{\text{obs}}|$.

¶ The analysis of the Ramachandran plot was done using PROCHECK²⁹.

the tunable bending magnet beamline X31 where the wavelength was adjusted to maximize the anomalous signal from the heavy atoms. In all experiments, only one crystal was needed for a complete set. A single native crystal was flash-frozen after being transferred to a cryoprotectant solution of 30% glycerol in the crystallization medium. The unit cell dimensions after freezing were $a = b = 81.3 \text{ \AA}$, $c = 72.6 \text{ \AA}$. Data were reduced and scaled using the HKL package containing DENZO and SCALEPACK programs (Z. Otwinowski and W. Minor). Unless specified otherwise, all software was used as implemented in the CCP4 suite of programs (Daresbury Laboratory, SERC, UK). Phases for room-temperature data were refined using MLPHARE and further enhanced using density modification, as implemented in SQUASH²⁷. The resulting map was of sufficient quality to allow 50% of the main-chain to be traced as polyaniline. This partial model was used in combination in SIGMAA (R. Read) to improve the phasing. The structure was traced using program O (ref. 28) and the model was refined at 2.1 Å resolution using PROLSQ, initially with residues 5–219. Water molecules were then added and refinement was continued with 13 residues (53–65) deleted from the model owing to intrinsic disorder in that region. When the 1.7 Å data were introduced, the orientation of the molecule was optimized using AMORE (J. Navaza) and X-PLOR (A. Brunger) version 3.1; only a small deviation in rotation and translation parameters was observed; the resulting *R*-factor for this model against all data was 0.33. A parallel calculation was done using only 90% of data to monitor the R_{free} value for 10% of randomly chosen reflections. The 2.1 Å model was subjected directly to two rounds of slow cooling using X-PLOR, followed by PROLSQ and REFMAC refinement of positional and thermal parameters; no manual revision of the model was done. As a result, the *R* factor was reduced for a model including 141 water molecules to 0.22, while the R_{free} was 0.27. At this point, refinement using all data was resumed at the point at which it was left. Several cycles of PROLSQ reduced the *R* factor to below 0.20. A number of side chains were corrected manually in program O and the acetate, now clearly defined in the active site, was included in the refinement. Of the 13 residues deleted from the previous model, only 4 had to be modelled into ambiguous density. The C-terminal amino acids 216–219 were deleted owing to the absence of interpretable density. Solvent structure and the model (consisting of residues 5–216, an acetate ion bound in the active site, and 241 water molecules) were refined using REFMAC, a maximum-likelihood refinement program. Because of the partial disorder of residues 55–61, their stereochemistry was relatively poor. A final refinement calculation was therefore done for a $\Delta 55\text{--}61$ model from which they were deleted. Stereochemical parameters for both models are listed in Table 1.

Received 3 September; accepted 4 November 1996.

- Venable, M. E., Zimmerman, G. A., McIntyre, T. M. & Prescott, S. M. *J. Lipid Res.* **34**, 691–702 (1993).
- O'Flaherty, J. T. & Wykle, R. L. in *Platelet Activating Factor and Human Disease* (eds Barnes, P. J., Page, C. P. & Henson, P.) 117–137 (Blackwell Scientific, Oxford, 1989).
- El Azzouzi, B., Jurgens, P., Benevise, P. & Thomas, Y. *Biochem. Biophys. Res. Commun.* **190**, 320–324 (1993).
- Shukla, D. *FASEB J.* **6**, 2296–2301 (1992).
- Bennett, S. A., Leite, L. C. & Birnboim, H. C. *Carcinogenesis* **14**, 1289–1296 (1993).
- Stafforini, D. M., Prescott, S. M., Zimmerman, G. A. & McIntyre, T. M. *Biochim. Biophys. Acta* **1301**, 161–173 (1996).
- Hattori, M., Adachi, H., Tsujimoto, M., Arai, H. & Inoue, K. *J. Biol. Chem.* **269**, 23150–23155 (1994).
- Hattori, M., Adachi, H., Tsujimoto, M., Arai, H. & Inoue, K. *Nature* **370**, 216–218 (1994).
- Hattori, M. et al. *J. Biol. Chem.* **270**, 31345–31352 (1995).
- Bazan, N. G. & Rodriguez de Turco, E. B. *Neurochem. Intern.* **26**, 435–441 (1995).
- Kumar, R., Harvey, S., Kester, N., Hanahan, D. & Olson, M. *Biochim. Biophys. Acta* **963**, 375–383 (1988).
- Panetta, T., Marcheselli, V. L., Braquet, P., Spinnewyn, B. & Bazan, N. G. *Biochem. Biophys. Res. Commun.* **149**, 580–587 (1987).
- Kato, K., Clark, G. D., Bazan, N. G. & Zorumski, D. F. *Nature* **367**, 175–179 (1994).
- Reiner, O. et al. *Nature* **364**, 717–721 (1993).
- Derewenda, Z. S. & Wei, Y. *J. Am. Chem. Soc.* **117**, 2104–2105 (1995).
- Tjoelker, L. W. et al. *J. Biol. Chem.* **270**, 25481–25487 (1995).
- Derewenda, Z. S. *Adv. Prot. Chem.* **45**, 1–52 (1994).
- Stremier, K. E., Stafforini, D. M., Prescott, S. M. & McIntyre, T. M. *J. Biol. Chem.* **266**, 11095–11103 (1991).
- Hattori, K. et al. *J. Biol. Chem.* **270**, 22308–22313 (1995).
- Sondek, J., Bohm, A., Lambright, D. G., Hamm, H. E. & Sigler, P. B. *Nature* **379**, 369–374 (1996).
- Hattori, M., Arai, H. & Inoue, K. *J. Biol. Chem.* **268**, 18748–18753 (1993).
- Reiner, O. et al. *J. Neurosci.* **15**, 3730–3738 (1995).
- Mizuguchi, M., Takashima, S., Kakita, A., Yamada, M. & Ikeda, K. *Am. J. Path.* **147**, 1142–1151 (1995).
- Xiang, X., Osmani, A. H., Osmani, S. A., Xin, M. & Morris, N. R. *Mol. Biol. Cell* **6**, 297–310 (1995).
- Wang, D. S. et al. *Biochem. Biophys. Res. Commun.* **209**, 622–629 (1995).
- Adachi, H., Tsujimoto, M., Hattori, M., Arai, H. & Inoue, K. *Biochem. Biophys. Res. Commun.* **214**, 180–187 (1995).
- Zhang, K. Y. *J. Acta Crystallogr. D* **49**, 213–222 (1993).
- Jones, T. A., Zou, J.-Y., Cowan, S. W. & Kjeldgaard, M. *Acta Crystallogr. A* **47**, 110–119 (1991).
- Laskowski, R. A., McArthur, M. W., Moss, D. S. & Thornton, J. M. *J. Appl. Crystal.* **20**, 282–291 (1993).
- Nicholls, A., Sharp, K. & Honig, B. *Proteins* **11**, 281–296 (1991).

CORRESPONDENCE and requests for materials should be addressed to Z.S.D. (e-mail: zsd4n@virginia.edu). Atomic coordinates have been deposited in the Brookhaven Protein Data Bank, entry code 1WAB, where they will be held for a year before release.